End-to-End Feasible Optimization Proxies for Large-Scale Economic Dispatch

Wenbo Chen, *Student Member, IEEE*, Mathieu Tanneau, and Pascal Van Hentenryck, *Member, IEEE*

***Abstract*—The article proposes a novel End-to-End Learning and Repair (E2ELR) architecture for training optimization proxies for economic dispatch problems. E2ELR combines deep neural networks with closed-form, differentiable repair layers, thereby integrating learning and feasibility in an end-to-end fashion. E2ELR is also trained with self-supervised learning, removing the need for labeled data and the solving of numerous optimization problems offline. E2ELR is evaluated on industry-size power grids with tens of thousands of buses using an economic dispatch that co-optimizes energy and reserves. The results demonstrate that the self-supervised E2ELR achieves state-of-the-art performance, with optimality gaps that outperform other baselines by at least an order of magnitude.**

***Index Terms*—Deep learning, economic dispatch, optimization proxies.**

Nomenclature

A. Sets and Indices

$i \in \mathcal{N}$	buses.
$e \in \mathcal{E}$	branches.
$g \in \mathcal{G}$	generators.

B. Variables

p_g	Energy dispatch of generator g.
r_g	Reserve dispatch of generator g.
ξ_e	Thermal limit violation on branch e.

C. Parameters

d_i	Active power demand at bus i.
c_g	Production cost function of generator g.
$\underline{f}_e, \bar{f}_e$	Lower and upper thermal limits on branch e.
M_{th}	Thermal violation penalty cost.
$\bar{p}_g$	Maximum output of generator g.
$\bar{r}_g$	Maximum reserve of generator g.
R	Minimum reserve requirement.
Φ	PTDF matrix.
$\mathbf{0}$	Vector of all zeros.
$\mathbf{e}$	Vector of all ones.

Manuscript received 24 April 2023; revised 18 August 2023; accepted 9 September 2023. Date of publication 20 September 2023; date of current version 21 February 2024. This work was supported in part by NSF under Grant 2007095 and Grant 2112533, and in part by ARPA-E PERFORM under Grant AR0001136. Paper no. TPWRS-00593-2023. *(Corresponding author: Mathieu Tanneau.)*

The authors are with the H. Milton Stewart School of Industrial and Systems Engineering, Georgia Institute of Technology, Atlanta, GA 30313 USA (e-mail: wenbo.chen@gatech.edu; mathieu.tanneau@isye.gatech.edu; pascal.vanhentenryck@isye.gatech.edu).

Color versions of one or more figures in this article are available at https://doi.org/10.1109/TPWRS.2023.3317352.

Digital Object Identifier 10.1109/TPWRS.2023.3317352

I. Introduction

The optimal power flow (OPF) is a fundamental problem in power systems operations. Its linear approximation, the DC-OPF model, underlies most electricity markets, especially in the US. For instance, MISO uses a security-constrained economic dispatch (SCED) in their real-time markets, which has the DC-OPF model at its core [1]. The continued growth in renewable and distributed energy resources (DERs) has caused an increase in operational uncertainty. This creates need for new methodologies and operating practices that can quantify and manage risk in real time [2], [3]. Nevertheless, quantifying the operational risk of a transmission system requires executing in the order of 10^3 Monte Carlo (MC) simulations, each requiring the solution of multiple (typically in the hundreds) economic dispatch problems [3], [4]. To fit within the constraints of actual operations, real-time risk assessment would thus require solving hundreds of thousands of economic dispatch problems within a matter of seconds. This represents a 100,000x speedup over current optimization technology, which can typically solve economic dispatch problems in a few seconds.

In recent years, there has been a surge of interest, both from the power systems and Machine-Learning (ML) communities, in developing optimization proxies for OPF, i.e., ML models that approximate the input-output mapping of OPF problems. The main idea is that, once trained, these proxies can be used to generate high-quality solutions orders of magnitude faster than traditional optimization solvers. This capability allows to evaluate a large number of scenarios fast, thereby enabling real-time risk assessment.

There are however three major obstacles to the deployment of optimization proxies: feasibility, scalability and adaptability. First, ML models are not guaranteed to satisfy the physical and engineering constraints of the model. This causes obvious issues if, for instance, the goal is to use a proxy to evaluate whether the system is able to operate in a safe state. Several approaches have been proposed in the past to address the feasibility of ML predictions, each of which has some advantages and limitations. Second, most results in ML for power systems has considered systems with up to 300 buses, far from the size of actual systems that contain thousands of buses. Moreover, the resulting techniques have not been proven to scale or be accurate enough on large-scale networks. Third, power grids are not static: the generator commitments and the grid topology evolve over time, typically on an hourly basis [5]. Likewise, the output of renewable generators such as wind and solar generators is non-stationary, which may degrade the performances of ML models. Therefore, it is important to be able to (re)train models fast, typically within a few hours at most. This obviously creates a computational bottleneck for approaches that rely on the offline solving of numerous optimization problems to generate training data.

Despite significant interest from the community, no approach has thus far addressed all three challenges (feasibility, scalability and adaptability) in a unified way. This article addresses this gap by proposing an *End-to-End Learning and Repair* (E2ELR) architecture for a (MISO-inspired) economic dispatch (ED) formulation where the prediction and feasibility restoration are integrated in a single ML pipeline and trained jointly. The E2ELR-ED architecture guarantees feasibility, i.e., it always outputs a feasible solution to the economic dispatch. The E2ELR-ED architecture achieves these results through *closed-form repair layers*. Moreover, through the use of *self-supervised learning*, the E2ELR-ED architecture is scalable, both for training and inference, and is found to produce near-optimal solutions to systems with tens of thousands of buses. Finally, the use of self-supervised learning also avoids the costly data-generation process of supervised-learning methods. This allows to re-train the model fast, smoothly adapting to changing operating parameters and system conditions. The contributions of the article can therefore be summarized as follows:

- The article proposes a novel E2ELR architecture with closed-form, differentiable repair layers, whose output is guaranteed to satisfy power balance and reserve requirements. This is the first architecture to consider reserve requirements, and to offer feasibility guarantees without restrictive assumptions.
- The E2ELR model is trained in an end-to-end fashion that combines learning and feasibility restoration, making the approach scalable to large-scale systems. This contrasts to traditional approaches that restore feasibility at inference time, which increases computing time and induces significant losses in accuracy.
- The article proposes self-supervised learning to eliminate the need for offline generation of training data. The proposed E2ELR can thus be trained from scratch in under an hour, even for large systems. This allows to adapt to changing system conditions by re-training the model periodically.
- The article conducts extensive numerical experiments on systems with up to 30,000 buses, a 100x increase in size compared to most existing studies. The results demonstrate that the proposed self-supervised E2ELR architecture is highly scalable and outperforms other approaches.

The rest of the article is organized as follows. Section II surveys the relevant literature. Section III presents an overview of the E2ELR architecture and contrast it with existing approaches. Section IV presents the problem formulation and the E2ELR architecture in detail. Section V presents supervised and self-supervised training. Section VI describes the experiment setting, and Section VII reports numerical results. Section VIII concludes the article and discusses future research directions.

II. Related Works

A. Optimization Proxies for OPF

The majority of the existing literature on OPF proxies employs Supervised Learning (SL) techniques. Each data point (x, y) consists of an OPF instance data (x) and its corresponding solution (y). The training data is obtained by solving a large number –usually tens of thousands– of OPF instances offline. The SL paradigm has successfully been applied both in the linear DCOPF [5], [6], [7], [8], [9], [10], [11] and nonlinear, non-convex ACOPF [12], [13], [14], [15], [16], [17], [18], [19], [20], [21], [22], [23], [24], [25], [26], [27], [28], [29] settings. In almost all the above references, the generator commitments and grid topology are assumed to be fixed, with electricity demand being the only source of variability. Therefore, these OPF proxies must be re-trained regularly to capture the hourly changes in commitments and topology that occur in real-life operations [5]. In a SL setting, this comes at a high computational cost because of the need to re-generate training data. Recent works consider active sampling techniques to reduce this burden [30], [31]. In [14], [24], [25], [26] consider graph neural network (GNN) architectures to accommodate topology changes, however, numerical results are only reported on small networks with at most 300 buses.

Self-Supervised Learning (SSL) has emerged as an alternative to SL that does not require labeled data [32], [33], [34]. Namely, training OPF proxies in a self-supervised fashion does *not* require the solving of any OPF instance offline, thereby removing the need for (costly) data generation. In [32], the authors train proxies for ACOPF where the training loss consists of the objective value of the predicted solution, plus a penalty term for constraint violations. A similar approach is used in [33] in conjunction with Generative Adversarial Networks (GANs). More recently, Park et al. [34] jointly train a primal and dual network by mimicking an Augmented Lagrangian algorithm. Predicting Lagrange multipliers allows for dynamically adjusting the constraint violation penalty terms in the loss function. Current results suggest that SSL-based proxies can match the accuracy of SL-based proxies.

B. Ensuring Feasibility

One major limitation of ML-based OPF proxies is that, in general, the predicted OPF solution violates physical and engineering constraints that govern power flows and ensure safe operations. To alleviate this issue, [9], [13] use a restricted OPF formulation to generate training data, wherein the OPF feasible region is artificially shrunk to ensure that training data consists of interior solutions. In [9], this strategy is combined with a verification step (see also [35]) to ensure the trained models have sufficient capacity to reach a universal approximation. Nevertheless, this requires solving bilevel optimization problems, which is very cumbersome: [9] reports training times in excess of week for a 300-bus system. In addition, it may not be possible to shrink the feasible region in general, e.g., when the lower and upper bounds are the same.

In the context of DCOPF, [5], [6], [10], [11] exploit the fact that an optimal solution can be quickly recovered from an (optimal) active set of constraints. A combined classification-then-regression architecture is proposed in [5], wherein a classification step identifies a subset of variables to be fixed to their lower or upper bound, thus reducing the dimension of the regression task. In [6], [11], the authors predict a full active set, and recover a solution by solving a system of linear equations. Similarly, [10] combine decision trees and active set-based affine policies. Importantly, active set-based approaches may yield infeasible solutions when active constraints are incorrectly classified [11]. Furthermore, correctly identifying an optimal active set becomes harder as problem size increases.

A number of prior work have investigated physics-informed models (e.g., [5], [13], [15], [16], [18], [19], [32], [33]). This approach augments the training loss function with a term that penalizes constraint violations, and is efficient at reducing – but not eliminating – constraint violations. To better balance feasibility and [15], [16] dynamically adjust the penalty coefficient using ideas from Lagrangian duality. In a similar fashion, [34] uses a primal and a dual networks: the latter predicts optimal Lagrange multipliers, which inform the loss function used to train the former.

Although physics-informed models generally exhibit lower constraint violations, they still do not produce feasible solutions. Therefore, several works combine an (inexact) OPF proxy with a repair step that restores feasibility. A projection step is used in [7], [15], wherein the (infeasible) predicted solution is projected onto the feasible set of OPF. In DCOPF, this projection is a convex (typically linear or quadratic) problem, whereas the load flow model used in [15] for ACOPF is non-convex. Instead of a projection step, [13] uses an AC power flow solver to recover voltage angles and reactive power dispatch from predicted voltage magnitudes and generator dispatches. This is typically (much) faster than a load flow. However, while the resulting solution satisfies the power flow equations (assuming the solver converges), it may not satisfy all engineering constraints such as the thermal limits of the lines. Finally, [36] uses techniques from state estimation to restore feasibility for ACOPF problems. This approach has not been applied in the context of OPF proxies.

The development of implicit differentiable layers [37] makes it possible to embed feasibility restoration inside the proxy architecture itself, thereby removing the need for post-processing [17], [38], [39]. This allows to train models in an *end-to-end* fashion, i.e., the predicted solution is guaranteed to satisfy constraints. For instance, [38] implement the aforementioned projection step as an implicit layer. However, because they require solving an optimization problem, these implicit layers incur a very high computational cost, both during training and testing. Equality constraints can also be handled implicitly via so-called constraint completion [17], [39]. Namely, a set of independent variables is identified, and dependent variables are recovered by solving the corresponding system of equations, thereby satisfying equality constraints by design. Note that constraint completion requires the set of independent variables to be the same across all instances, which may not hold in general. For instance, changes in generator commitments and/or grid topology may introduce dependencies between previously-independent variables. The difference between [17] and [39] lies in the treatment of inequality constraints. On the one hand, [17] replace a costly implicit layer with cheaper gradient unrolling, which unfortunately does not guarantee feasibility. On the other hand, [39] use gauge functions to define a one-to-one mapping between the unit hypercube, which is easy to enforce with sigmoid activations, and the set of feasible solutions, thereby guaranteeing feasibility. Nevertheless, the latter approach is valid only under restrictive assumptions: all constraints are convex, the feasible set is bounded, and a strictly feasible point is available for each instance.

C. *Scalability Challenges*

There exists a significant gap between the scale of actual power grids, and those used in most academic studies: the former are typically two orders of magnitude larger than the latter. On the one hand, actual power grids comprise thousands to tens of thousands of buses [40], [41]. On the other hand, most academic studies only consider small, artificial power grids with no more than 300 buses. Among the aforementioned works, [11] considers a synthetic NYISO grid with 1814 buses, and only [5], [16], [27] report results on systems with more than 6,000 buses. This discrepancy makes it difficult to extrapolate most existing findings to scenarios encountered in the industry. Indeed, actual power grids exhibit complex behaviors not necessarily captured by small-scale cases [40].

III. Overview of the Proposed Approach

The article addresses the shortcomings in current literature by combining learning and feasibility restoration in a single E2ELR architecture. Fig. 1 illustrates the proposed architecture (Fig. 1(e)), alongside existing architectures from previous works. In contrast to previous works, the proposed E2ELR uses specialized, closed-form repair layers that allow the architecture to scale to industry-size systems. E2ELR is also trained with self-supervised learning, alleviating the need for labeled data and the offline solving of numerous optimization problems. As a result, even for the largest systems considered, the self-supervised E2ELR is trained from scratch in under an hour, and achieves state-of-the-art performance, outperforming other baselines by an order of magnitude. Note that E2ELR also bridges the gap between academic DCOPF formulations and those used in the industry, by including reserve requirements in the ED formulation. To the best of the authors' knowledge, this is the first work to explicitly consider –and offer feasibility guarantees for– reserve requirements in the context of optimization proxies. Moreover, the repair layers are guaranteed to satisfy power balance and reserve requirements for any combination of min/max generation limits (see Theorems 1 and

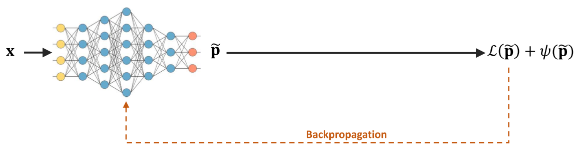

(a) The vanilla DNN architecture without feasibility restoration.

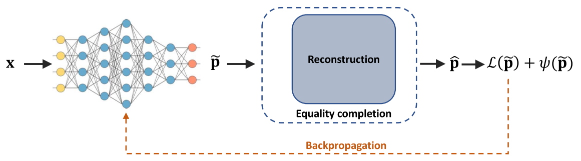

(b) The DeepOPF architecture [7]. The output $\hat{\mathbf{p}}$ may violate inequality constraints.

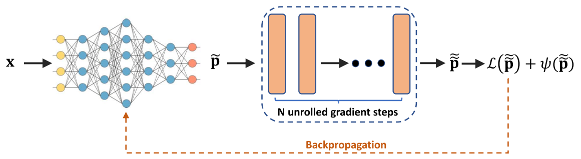

(c) The DC3 architecture with unrolled gradient [17]. The output $\tilde{\mathbf{p}}$ may violate inequality constraints.

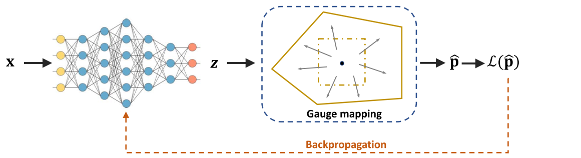

(d) The LOOP-LC architecture [39]. The DNN outputs a latent vector $\mathbf{z} \in [0,1]^n$, which is mapped onto a feasible $\hat{\mathbf{p}}$ via a gauge mapping.

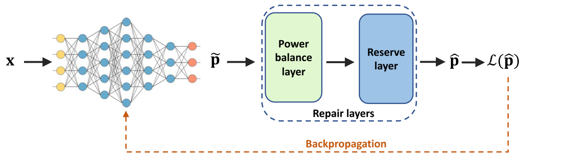

(e) The proposed end-to-end feasible architecture. The output $\hat{\mathbf{p}}$ satisfies all hard constraints.

Fig. 1. Optimization proxy architectures for DCOPF.

2). This allows to accommodate variations in operating parameters such as min/max limits and commitment status of generators, a key aspect of real-life systems overlooked in existing literature.

IV. End-to-End Feasible Proxies for DCOPF

This section presents the Economic Dispatch (ED) formulation considered in the article, and introduces new repair layers for power balance and reserve requirement constraints. The repair layers are computationally efficient and differentiable: they can be implemented in standard machine-learning libraries, enabling end-to-end feasible optimization proxies.

A. Problem Formulation

The article considers an ED formulation with reserve requirements. It is modeled as a linear program of the form

$$\min_{\mathbf{p},\mathbf{r},\xi_{\text{th}}} \quad c(\mathbf{p}) + M_{\text{th}}\|\xi_{\text{th}}\|_1 \tag{1a}$$

$$\text{s.t.} \quad \mathbf{e}^\top \mathbf{p} = \mathbf{e}^\top \mathbf{d}, \tag{1b}$$

$$\mathbf{e}^\top \mathbf{r} \geq R, \tag{1c}$$

$$\mathbf{p} + \mathbf{r} \leq \bar{\mathbf{p}}, \tag{1d}$$

$$\mathbf{0} \leq \mathbf{p} \leq \bar{\mathbf{p}}, \tag{1e}$$

$$\mathbf{0} \leq \mathbf{r} \leq \bar{\mathbf{r}}, \tag{1f}$$

$$\underline{\mathbf{f}} - \xi_{\text{th}} \leq \Phi(\mathbf{p} - \mathbf{d}) \leq \bar{\mathbf{f}} + \xi_{\text{th}}, \tag{1g}$$

$$\xi_{\text{th}} \geq \mathbf{0}. \tag{1h}$$

Constraints (1b) and (1c) are the global power balance and minimum reserve requirement constraints, respectively. Constraints (1d) ensure that each generator reserves can be deployed without violating their maximum capacities. Constraints (1e) and (1f) enforce minimum and maximum limits on each generator energy and reserve dispatch. Without loss of generality, the article assumes that each bus has exactly one generator, each generator minimum output is zero, and $\bar{r}_g \leq \bar{p}_g, \forall g$. Constraints (1g) express the thermal constraints on each branch using a Power Transfer Distribution Factor (PTDF) representation. In this article, the thermal constraints are soft constraints, i.e., they can be violated but doing so incurs a (high) cost. This is modeled via artificial slack variables ξ_{th} which are penalized in the objective. Treating thermal constraints as soft is in line with economic dispatch formulations used by system operators to clear electricity markets in the US [42], [43]. The PTDF-based formulation is also the state-of-the-art approach used in industry [41], [42]. In typical operations, only a small number of these constraints are active at the optimum. Therefore, efficient implementations add thermal constraints (1g) lazily.

The hard constraints in Problem (1) are the bounds on energy and reserve dispatch, the maximum output, the power balance (1b) and the reserve requirements (1c). Note that bounds on individual variables can easily be enforced in a DNN architecture e.g., via clamping or sigmoid activation. However, it is not trivial to *simultaneously* satisfy variable bounds, power balance and reserve requirements. To address this issue, the rest of this section introduces new, computationally efficient repair layers.

B. The Power Balance Repair Layer

The proposed power balance repair layer takes as input an initial dispatch vector $\mathbf{p}$, which is assumed to satisfy the min/max generation bounds (1e), and outputs a dispatch vector $\tilde{\mathbf{p}}$ that satisfies constraints (1e) and (1b). Formally, let $D = \mathbf{e}^\top \mathbf{d}$, and denote by $\mathcal{H}$ and $\mathcal{S}_D$ the following hypercube and hypersimplex

$$\mathcal{H} = \left\{\mathbf{p} \in \mathbb{R}^n \mid \mathbf{0} \leq \mathbf{p} \leq \bar{\mathbf{p}}\right\}, \tag{2}$$

$$\mathcal{S}_D = \left\{\mathbf{p} \in \mathbb{R}^n \mid \mathbf{0} \leq \mathbf{p} \leq \bar{\mathbf{p}},\ \mathbf{e}^\top \mathbf{p} = D\right\}. \tag{3}$$

Note that $\mathcal{H}$ is the feasible set of constraints (1e), while $\mathcal{S}_D$ is the feasible set of constraints (1b) and (1e). The proposed power balance repair layer, denoted by $\mathcal{P}$, is given by

$$\mathcal{P}(\mathbf{p}) = \begin{cases} (1-\eta^\uparrow)\mathbf{p} + \eta^\uparrow \bar{\mathbf{p}} & \text{if } \mathbf{e}^\top \mathbf{p} < D \\ (1-\eta^\downarrow)\mathbf{p} + \eta^\downarrow \mathbf{0} & \text{if } \mathbf{e}^\top \mathbf{p} \geq D \end{cases} \tag{4}$$

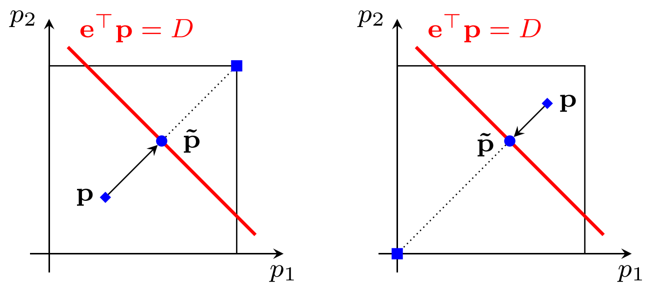

Fig. 2. Illustration of the power balance layer with input $\mathbf{p}$ and output $\tilde{\mathbf{p}}$. Left: $\mathbf{e}^\top\mathbf{p} < D$ (energy shortage) and generators' dispatches are increased. Right: $\mathbf{e}^\top\mathbf{p} > D$ (energy surplus) and generators' dispatches are decreased.

where $\mathbf{p} \in \mathcal{H}$, and $\eta^\uparrow$, $\eta^\downarrow$ are defined as follows:

$$\eta^\uparrow = \frac{\mathbf{e}^\top\mathbf{d} - \mathbf{e}^\top\mathbf{p}}{\mathbf{e}^\top\bar{\mathbf{p}} - \mathbf{e}^\top\mathbf{p}}, \qquad \eta^\downarrow = \frac{\mathbf{e}^\top\mathbf{p} - \mathbf{e}^\top\mathbf{d}}{\mathbf{e}^\top\mathbf{p} - \mathbf{e}^\top\mathbf{0}}. \tag{5}$$

Theorem 1 below shows that $\mathcal{P}$ is well-defined.

Theorem 1: Assume that $0 < \mathbf{e}^\top\mathbf{d} = D < \mathbf{e}^\top\bar{\mathbf{p}}$ and $\mathbf{p} \in \mathcal{H}$. Then, $\mathcal{P}(\mathbf{p}) \in \mathcal{S}_D$.

Proof: Let $\tilde{\mathbf{p}} = \mathcal{P}(\mathbf{p})$, and assume $\mathbf{e}^\top\mathbf{p} < D$; the case $\mathbf{e}^\top\mathbf{p} \geq D$ is treated similary. It follows that $\eta^\uparrow \in [0,1]$, i.e., $\tilde{\mathbf{p}}$ is a convex combination of $\mathbf{p}$ and $\bar{\mathbf{p}}$. Thus, $\tilde{\mathbf{p}} \in \mathcal{H}$. Then,

$$\begin{aligned}
\mathbf{e}^\top\tilde{\mathbf{p}} &= (1-\eta^\uparrow)\mathbf{e}^\top\mathbf{p} + \eta^\uparrow\mathbf{e}^\top\bar{\mathbf{p}} \\
&= \eta^\uparrow(\mathbf{e}^\top\bar{\mathbf{p}} - \mathbf{e}^\top\mathbf{p}) + \mathbf{e}^\top\mathbf{p} \\
&= \frac{D - \mathbf{e}^\top\mathbf{p}}{\mathbf{e}^\top\bar{\mathbf{p}} - \mathbf{e}^\top\mathbf{p}}(\mathbf{e}^\top\bar{\mathbf{p}} - \mathbf{e}^\top\mathbf{p}) + \mathbf{e}^\top\mathbf{p} \\
&= D - \mathbf{e}^\top\mathbf{p} + \mathbf{e}^\top\mathbf{p} = D.
\end{aligned}$$

Thus, $\tilde{\mathbf{p}}$ satisfies the power balance and $\tilde{\mathbf{p}} \in \mathcal{S}_D$. □

Note that feasible predictions are not modified: if $\mathbf{p} \in \mathcal{S}_D$, then $\mathcal{P}(\mathbf{p}) = \mathbf{p}$. The edge cases not covered by Theorem 1 are handled as follows. When $D \leq 0$ (resp. $D \geq \mathbf{e}^\top\bar{\mathbf{p}}$), each generator is set to its lower (resp. upper) bound; this can be achieved by clamping $\eta^\uparrow$ (resp. $\eta^\downarrow$) to $[0,1]$. If these inequalities are strict, Problem (1) is trivially infeasible, and $\mathcal{P}(\mathbf{p})$ is the solution that minimizes power balance violations.

The power balance layer is illustrated in Fig. 2, for a two-generator system. The layer has an intuitive interpretation as a proportional response mechanism. Indeed, if the initial dispatch $\mathbf{p}$ has an energy shortage, i.e., $\mathbf{e}^\top\mathbf{p} < D$, the output of each generator is increased by a fraction $\eta^\uparrow$ of its upwards headroom. Likewise, if the initial dispatch has an energy surplus, i.e., $\mathbf{e}^\top\mathbf{p} > D$, the output of each generator is decreased by a fraction $\eta^\downarrow$ of it downwards headroom.

Note that $\mathcal{S}_D$ is defined by the combination of bound constraints and one equality constraint. Other works such as [17], [39] handle the latter via equality completion. While this approach satisfies the equality constraint by design, the recovered solution is not guaranteed to satisfy min/max bounds, and may fail to do so in general. In contrast, under the only assumption that $\mathbf{p} \in \mathcal{H}$, the proposed layer (4) jointly enforces *both* constraints, thus alleviating the need for the gradient unrolling of [17] or gauge mapping of [39]. Finally, the proposed layer generalizes to hypersimplices of the form

$$\left\{x \in \mathbb{R}^n \mid l \leq x \leq u, a^T x = b\right\}, \tag{6}$$

where $a \in \mathbb{R}^n, b \in \mathbb{R}$ and $l \leq u \in \mathbb{R}^n$ are finite bounds.

C. The Reserve Repair Layer

This section presents the proposed reserve feasibility layer, which ensures feasibility with respect to constraints (1c), (1d), and (1f). The approach first builds a compact representation of these constraints by projecting out the reserve variables $\mathbf{r}$. This makes it possible to consider only the $\mathbf{p}$ variables, which in turn enables a computationally efficient and interpretable feasibility restoration. Let $\mathbf{p} \in \mathcal{S}_D$ be fixed, and consider the problem of maximizing total reserves, which reads

$$\max_{\mathbf{r}} \quad \mathbf{e}^\top\mathbf{r} \tag{7a}$$

$$\text{s.t.} \quad \mathbf{r} \leq \bar{\mathbf{p}} - \mathbf{p}, \tag{7b}$$

$$0 \leq \mathbf{r} \leq \bar{\mathbf{r}}. \tag{7c}$$

Since $\mathbf{p}$ is fixed, constraints (7b)–(7c) reduce to simple variable bounds on the $\mathbf{r}$ variables. It then immediately follows that the optimal solution to Problem (7) is given by

$$r_g^* = \min\{\bar{r}_g, \bar{p}_g - p_g\}, \ \forall g. \tag{8}$$

This observation is used to project out the reserve variables as stated in Lemma 1 below.

Lemma 1: Let $\mathbf{p} \in \mathcal{S}_D$. There exists reserves $\mathbf{r}$ such that $(\mathbf{p}, \mathbf{r})$ is feasible for Problem (1) if and only if

$$\sum_g \min\{\bar{r}_g, \bar{p}_g - p_g\} \geq R. \tag{9}$$

Proof: The proof follows from the fact that $(\mathbf{p}, \mathbf{r})$ is feasible for Problem (1) if and only if Problem (7) has an objective value not smaller than R. Substituting the optimal solution given in (8), this last statement is exactly equivalent to $\sum_g \min\{\bar{r}_g, \bar{p}_g - p_g\} \geq R$. □

The proposed reserve repair layer builds on the power balance repair layer of Section IV-B, and on the compact formulation of (9). Namely, it takes as input $\mathbf{p} \in \mathcal{S}_D$, and outputs $\mathcal{R}(\mathbf{p}) \in \mathcal{S}_D$ that satisfies (9). Given $\mathcal{R}(\mathbf{p})$, reserve variables can be recovered in $O(|\mathcal{G}|)$ time using (8).

The reserve repair layer is presented in Algorithm 1. First, a tentative reserve allocation is computed using (8), and the corresponding reserve shortage Δ_R is computed. Then, generators are split into two groups $\mathcal{G}^\uparrow$ and $\mathcal{G}^\downarrow$. Generators in $\mathcal{G}^\uparrow$ are those for which constraint (1f) is active: their dispatch can be increased without having to reduce their reserves. Generators in $\mathcal{G}^\downarrow$ are those for which constraint (1d) is active: one must reduce their energy dispatch to increase their reserves. Then, the algorithm computes the maximum possible increase ($\Delta^\uparrow$) and decrease ($\Delta^\downarrow$) in energy dispatch for the two groups. Finally, each generator energy dispatch is increased (resp. decreased) proportionately to its increase (resp. decrease) potential so as to meet total reserve requirements. The total increase in energy dispatch is equal to the total decrease, so that power balance is always maintained.

Algorithm 1: Reserve Repair Layer.

```
Require: Initial prediction $\mathbf{p} \in \mathcal{S}_D$, maximum limits $\bar{\mathbf{p}}, \bar{\mathbf{r}}$,
    reserve requirement $R$
1: $\Delta_R \leftarrow R - \sum_g \min\{\bar{r}_g, \bar{p}_g - p_g\}$
2: $\mathcal{G}^{\uparrow} \leftarrow \{g \mid p_g \leq \bar{p}_g - \bar{r}_g\}$
3: $\mathcal{G}^{\downarrow} \leftarrow \{g \mid p_g > \bar{p}_g - \bar{r}_g\}$
4: $\Delta^{\uparrow} \leftarrow \sum_{g \in \mathcal{G}^{\uparrow}} (\bar{p}_g - \bar{r}_g) - p_g$
5: $\Delta^{\downarrow} \leftarrow \sum_{g \in \mathcal{G}^{\downarrow}} p_g - (\bar{p}_g - \bar{r}_g)$
6: $\Delta \leftarrow \max(0, \min(\Delta_R, \Delta^{\uparrow}, \Delta^{\downarrow}))$
7: $\alpha^{\uparrow} \leftarrow \Delta/\Delta^{\uparrow}$, $\alpha^{\downarrow} \leftarrow \Delta/\Delta^{\downarrow}$,
8: Energy dispatch adjustment
    $\tilde{p}_g = \begin{cases} (1-\alpha^{\uparrow})p_g + \alpha^{\uparrow}(\bar{p}_g - \bar{r}_g) & \forall g \in \mathcal{G}^{\uparrow} \\ (1-\alpha^{\downarrow})p_g + \alpha^{\downarrow}(\bar{p}_g - \bar{r}_g) & \forall g \in \mathcal{G}^{\downarrow} \end{cases}$
9: return $\mathcal{R}(\mathbf{p}) = \tilde{\mathbf{p}}$
```

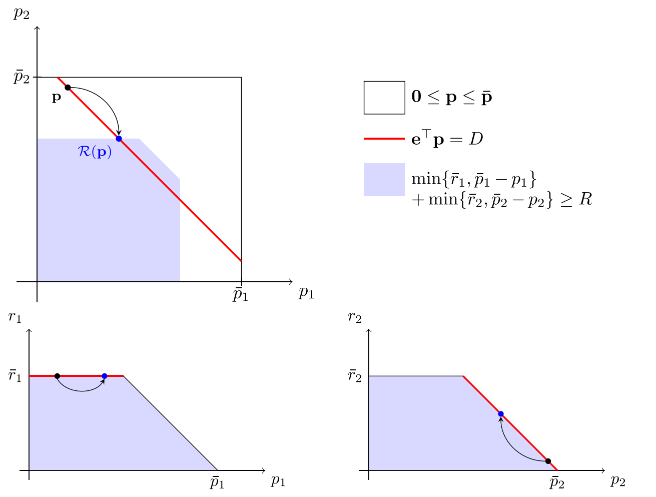

Fig. 3. Illustration of the reserve feasibility layer for $\bar{\mathbf{p}} = (1, 1)$, $\bar{\mathbf{r}} = (0.5, 0.5)$, $D = 1.1$, $R = 0.8$ and the initial prediction $\mathbf{p} = (0.15, 0.95)$. The recovered feasible dispatch is $\tilde{\mathbf{p}} = (0.4, 0.7)$. Top: effect of the layer in the (p_1, p_2) space. Bottom: effect of the layer on each generator (individually). The active constraint is shown in red. Generator 1 is in $\mathcal{G}^{\uparrow}$ and generator 2 is in $\mathcal{G}^{\downarrow}$.

The reserve feasibility recovery is illustrated in Fig. 3 for a two-generator system. While it is easy to verify that $\mathcal{R}(\mathbf{p}) \in \mathcal{S}_D$, it is less clear whether $\mathcal{R}(\mathbf{p})$ satisfies (9). Theorem 2 provides the theoretical guarantee that either $\mathcal{R}(\mathbf{p})$ satisfies (9), or no feasible solution to Problem (1) exists. Because of space limitations, the proof is given in [44].

Theorem 2: Let $\mathbf{p} \in \mathcal{S}_D$. Then, $\mathcal{R}(\mathbf{p}) \in \mathcal{S}_D$. Furthermore, $\mathcal{R}(\mathbf{p})$ satisfies (9) if and only if Problem (1) is feasible.

Theorem 2 also provides a fast proof of (in)feasibility for Problem (1): it suffices to evaluate $\mathcal{R}(\mathbf{p})$ for any $\mathbf{p} \in \mathcal{S}_D$ and check (9). This can have applications beyond optimization proxies, e.g., to quickly evaluate a large number of scenarios for potential reserve violations. Finally, note that the results of Theorems 1 and 2 hold for any value of the maximum limits $\bar{\mathbf{p}}, \bar{\mathbf{r}}$ and reserve requirement R.

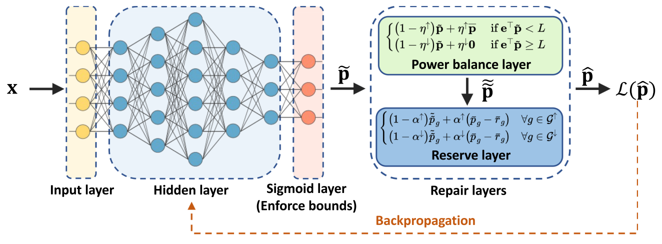

$\mathbf{x}$
Input layer
Hidden layer
Sigmoid layer (Enforce bounds)
$\tilde{\mathbf{p}}$
$\begin{cases} (1-\eta^{\uparrow})\tilde{\mathbf{p}} + \eta^{\uparrow}\bar{\mathbf{p}} & \text{if } \mathbf{e}^\top\tilde{\mathbf{p}} < L \\ (1-\eta^{\downarrow})\tilde{\mathbf{p}} + \eta^{\downarrow}\mathbf{0} & \text{if } \mathbf{e}^\top\tilde{\mathbf{p}} \geq L \end{cases}$
Power balance layer
$\tilde{\tilde{\mathbf{p}}}$
$\begin{cases} (1-\alpha^{\uparrow})\tilde{\tilde{p}}_g + \alpha^{\uparrow}(\bar{p}_g - \bar{r}_g) & \forall g \in \mathcal{G}^{\uparrow} \\ (1-\alpha^{\downarrow})\tilde{\tilde{p}}_g + \alpha^{\downarrow}(\bar{p}_g - \bar{r}_g) & \forall g \in \mathcal{G}^{\downarrow} \end{cases}$
Reserve layer
Repair layers
$\hat{\mathbf{p}}$
$\mathcal{L}(\hat{\mathbf{p}})$
Backpropagation

Fig. 4. Proposed end-to-end feasible architecture.

D. End-to-end Feasible Training

The repair layers are combined with a Deep Neural Network (DNN) architecture to provide an end-to-end feasible ML model, i.e., a differentiable architecture that is guaranteed to output a feasible solution to Problem (1) (if and only if one exists). The resulting architecture is illustrated in Fig. 4. The proxy takes as input the vector of nodal demand $\mathbf{d}$. The DNN architecture consists of fully-connected layers with ReLU activation, and a final layer with sigmoid activations to enforce bound constraints on $\mathbf{p}$. Namely, the last layer outputs $\mathbf{z} \in [0, 1]^n$, and $\tilde{\mathbf{p}} = \mathbf{z} \cdot \bar{\mathbf{p}}$ satisfies constraints (1e). Then, this initial prediction $\tilde{\mathbf{p}}$ is fed to the repair layers that restore the feasibility of the power balance and reserve requirements. The final prediction $\hat{\mathbf{p}}$ is feasible for Problem (1).

The power balance and reserve feasibility layers only require elementary arithmetic and logical operations, all of which are supported by mainstream ML libraries like PyTorch and TensorFlow. Therefore, it can be implemented as a layer of a generic artificial neural network model trained with back-propagation. Indeed, these layers are differentiable almost everywhere with informative (sub)gradients. Finally, the proposed feasibility layers can be used as a stand-alone, post-processing step to restore feasibility of any dispatch vector that satisfies generation bounds. This can be used for instance to build fast heuristics with feasibility guarantees.

V. Training Methodology

This section describes the supervised learning (SL) and self-supervised learning (SSL) approaches for training optimization proxies, which are illustrated in Fig. 5. The difference between these two paradigms lies in the choice of loss function for training, not in the model architecture. Denote by $\mathbf{x}$ the input data of Problem (1), i.e.,

$$\mathbf{x} = (c, \mathbf{d}, R, \bar{\mathbf{p}}, \bar{\mathbf{r}}, \Phi, \underline{\mathbf{f}}, \bar{\mathbf{f}}, M_{\text{th}}),$$

and recall, from Section IV-C, that it is sufficient to predict the (optimal) value of variables $\mathbf{p}$. Denote by f_θ the mapping of a DNN architecture with trainable parameters θ; given an input $\mathbf{x}$, $f_\theta(\mathbf{x})$ predicts a generator dispatch $f_\theta(\mathbf{x}) = \hat{\mathbf{p}}$.

Consider a dataset of N data points

$$\mathcal{D} = \left\{ \left(\mathbf{x}^{(1)}, \mathbf{p}^{(1)}\right), \ldots, \left(\mathbf{x}^{(N)}, \mathbf{p}^{(N)}\right) \right\}, \tag{10}$$

where each data point corresponds to an instance of Problem (1) and its solution, i.e., $\mathbf{x}^{(i)}$ and $\mathbf{p}^{(i)}$ denote the input data and

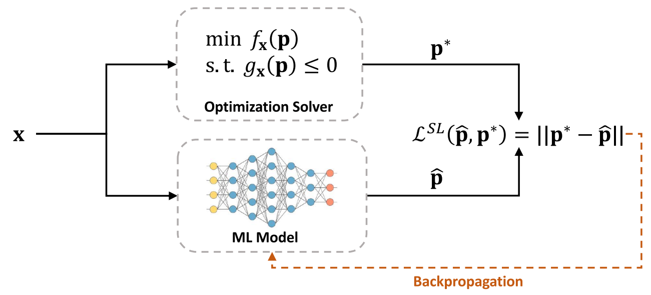
min $f_{\mathbf{x}}(\mathbf{p})$
s.t. $g_{\mathbf{x}}(\mathbf{p}) \le 0$
Optimization Solver
$\mathbf{p}^*$
$\mathbf{x}$
$\mathcal{L}^{SL}(\hat{\mathbf{p}}, \mathbf{p}^*) = ||\mathbf{p}^* - \hat{\mathbf{p}}||$
$\hat{\mathbf{p}}$
ML Model
Backpropagation

(a) Supervised Learning: the loss function $\mathcal{L}^{SL}$ measures the distance to an optimal solution $\mathbf{p}^*$, which is computed offline by an optimization solver.

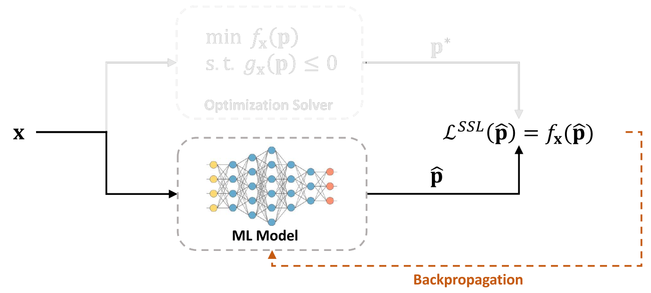
min $f_{\mathbf{x}}(\mathbf{p})$
s.t. $g_{\mathbf{x}}(\mathbf{p}) \le 0$
Optimization Solver
$\mathbf{p}^*$
$\mathbf{x}$
$\mathcal{L}^{SSL}(\hat{\mathbf{p}}) = f_{\mathbf{x}}(\hat{\mathbf{p}})$
$\hat{\mathbf{p}}$
ML Model
Backpropagation

(b) Self-Supervised Learning: the loss function $\mathcal{L}^{SSL}$ measures the objective value of the prediction. No target $\mathbf{p}^*$ nor optimization solver is needed.

Fig. 5. Illustration of supervised and self-supervised learning paradigms. When the ML model is not guaranteed to produce feasible solutions, the loss function $\mathcal{L}$ can be augmented with a constraint penalization term.

solution of instance $i \in \{1, \dots, N\}$, respectively. The training of the DNN f_θ can be formalized as the optimization problem

$$\theta^* = \underset{\theta}{\text{arg-min}} \quad \frac{1}{N} \sum_{i=1}^{N} \mathcal{L}\left(\hat{\mathbf{p}}^{(i)}, \mathbf{p}^{(i)}\right), \tag{11}$$

where $\hat{\mathbf{p}}^{(i)} = f_{\theta^*}(\mathbf{x}^{(i)})$ is the prediction for instance i, and $\mathcal{L}$ denotes the loss function. The rest of this section describes the choice of loss function $\mathcal{L}$ for the SL and SSL settings.

A. Supervised Learning

The supervised learning loss $\mathcal{L}^{\text{SL}}$ has the form

$$\mathcal{L}^{\text{SL}}(\hat{\mathbf{p}}, \mathbf{p}) = \varphi^{\text{SL}}(\hat{\mathbf{p}}, \mathbf{p}) + \lambda\psi(\hat{\mathbf{p}}), \tag{12}$$

where $\varphi^{\text{SL}}(\hat{\mathbf{p}}, \mathbf{p})$ penalizes the distance between the predicted and the target (ground truth) solutions, and $\psi(\hat{\mathbf{p}})$ penalizes constraint violations. The article uses the Mean Absolute Error (MAE) on energy dispatch, i.e.,

$$\varphi^{\text{SL}}(\hat{\mathbf{p}}, \mathbf{p}) = \frac{1}{|\mathcal{G}|}\|\hat{\mathbf{p}} - \mathbf{p}\|_1. \tag{13}$$

Note that other loss functions, e.g., Mean Squared Error (MSE), could be used instead. The term $\psi(\hat{\mathbf{p}})$ penalizes power balance violations and reserve shortages as follows:

$$\psi(\hat{\mathbf{p}}) = M_{\text{pb}}|\mathbf{e}^\top \mathbf{d} - \mathbf{e}^\top \hat{\mathbf{p}}| + M_{\text{r}}\xi_{\text{r}}(\hat{\mathbf{p}}), \tag{14}$$

where M_{pb} and M_{r} are penalty coefficients, and ξ_{r} denotes the reserve shortages, i.e.,

$$\xi_{\text{r}}(\hat{\mathbf{p}}) = \max\left\{0, R - \sum_{g} \min(\bar{r}_g, \bar{p}_g - \hat{p}_g)\right\}. \tag{15}$$

The penalty term ψ is set to zero for end-to-end feasible models. Finally, while thermal constraints are soft, preliminary experiments found that including thermal violations in the loss function yields more accurate models. This observation echoes the findings of multiple studies [6], [7], [8], [15], [17], namely, that penalizing constraint violations yields better accuracy and improves generalization. Indeed, the penalization of thermal violations acts as a regularizer in the loss function. Therefore, the final loss considered in the article is

$$\mathcal{L}^{\text{SL}}(\hat{\mathbf{p}}, \mathbf{p}) = \varphi^{\text{SL}}(\hat{\mathbf{p}}, \mathbf{p}) + \lambda\psi(\hat{\mathbf{p}}) + \mu M_{\text{th}}\|\xi_{\text{th}}(\hat{\mathbf{p}})\|_1, \tag{16}$$

where $\xi_{\text{th}}(\hat{\mathbf{p}})$ denotes thermal violations (1g).

B. Self-Supervised Learning

Self-supervised learning has been applied very recently to train optimization proxies [17], [32], [34]. The core aspect of SSL is that *it does not require the labeled data* $\mathbf{p}$, because it directly minimizes the objective function of the original problem. The self-supervised loss guides the training to imitate the solving of optimization instances using gradient-based algorithms, which makes it effective for optimization proxies.

The loss function $\mathcal{L}^{\text{SSL}}$ has the form

$$\mathcal{L}^{\text{SSL}}(\hat{\mathbf{p}}) = \varphi^{\text{SSL}}(\hat{\mathbf{p}}) + \lambda\psi(\hat{\mathbf{p}}), \tag{17}$$

where $\psi(\hat{\mathbf{p}})$ is the same as (14), and

$$\varphi^{\text{SSL}}(\hat{\mathbf{p}}) = c(\hat{\mathbf{p}}) + M_{\text{th}}\xi_{\text{th}}(\hat{\mathbf{p}}) \tag{18}$$

is the objective value of the predicted solution. As mentioned above, note that $\mathcal{L}^{SLL}$ only depends on the predicted solution $\hat{\mathbf{p}}$, i.e., unlike the supervised learning loss $\mathcal{L}^{SL}$ (see (16)), it does not require any ground truth solution $\mathbf{p}$. Consequently, SSL does not require labeled data. This, in turn, eliminates the need to solve numerous instances offline.

Again, the constraint penalty term is zero when training end-to-end feasible models, because their output satisfies all hard constraints. Thereby, the self-supervised loss is very effective since the learning focuses on optimality.

For models without feasibility guarantees, the trade-off between optimality and feasibility typically makes the training very hard to stabilize for large-scale systems, which increases the learning difficulty. Thus, such models must take care to satisfy constraints to avoid spurious solutions. For instance, in the ED setting, simply minimizing total generation cost, without considering the power balance constraint (1b), yields the trivial solution $\mathbf{p} = \mathbf{0}$. This highlights the importance of ensuring feasibility, which is the core advantage of the proposed end-to-end feasible architecture.

TABLE I
SELECTED TEST CASES FROM PGLIB [45]

System	Ref	$\|\mathcal{N}\|$	$\|\mathcal{E}\|$	$\|\mathcal{G}\|$	D_{ref}†	α_{r}
ieee300	[46]	300	411	69	23.53	34.16%
pegase1k	[40]	1354	1991	260	73.06	19.82%
rte6470	[40]	6470	9005	761	96.59	14.25%
pegase9k	[40]	9241	16049	1445	312.35	4.70%
pegase13k	[40]	13659	20467	4092	381.43	1.32%
goc30k	[47]	30000	35393	3526	117.74	4.68%

†Total active power demand in reference PGLib case, in GW.

VI. Experiment Settings

This section presents the numerical experiments used to assess E2ELR. The experiments are conducted on power grids with up to 30,000 buses and uses two variants of Problem 1 with and without reserve requirements. The section presents the data-generation methodology, the baseline ML architectures, performance metrics, and implementation details. Additional information is in [44].

A. Data Generation

Instances of Problem (1) are obtained by perturbing reference test cases from the PGLib [45] library (v21.07). Two categories of instances are generated: instances without any reserve requirements (ED), and instances with reserve requirements (ED-R). The instances are generated as follows. Denote by $\mathbf{d}^{\text{ref}}$ the nodal load vector from the reference PGLib case. ED instances are obtained by perturbing this reference load profile. Namely, for instance i, $\mathbf{d}^{(i)} = \gamma^{(i)} \times \eta^{(i)} \times \mathbf{d}^{\text{ref}}$, where $\gamma^{(i)} \in \mathbb{R}$ is a global scaling factor, $\eta \in \mathbb{R}^{|\mathcal{N}|}$ denotes load-level multiplicative white noise, and the multiplications are element-wise. For the case at hand, γ is sampled from a uniform distribution $U[0.8, 1.2]$, and, for each load, η is sampled from a log-normal distribution with mean 1 and standard deviation 5%.

ED-R instances are identical to the ED instances, except that reserve requirements are set to a non-zero value. The PGLib library does not include reserve information, therefore, the article assumes $\bar{r}_g = \alpha_{\text{r}} \bar{p}_g, \forall g \in \mathcal{G}$, where $\alpha_{\text{r}} = 5 \times \|\bar{\mathbf{p}}\|_\infty \times \|\bar{\mathbf{p}}\|_1^{-1}$. This ensures that the total reserve capacity is 5 times larger than the largest generator in the system. Then, the reserve requirements of each instance is sampled uniformly between 100% and 200% of the size of the largest generator, thereby mimicking contingency reserve requirements used in industry.

Table I presents the systems used in the experiments. The table reports: the number of buses ($|\mathcal{N}|$), the number of branches ($|\mathcal{E}|$), the number of generators ($|\mathcal{G}|$), the total active power demand in the reference PGLib case (D_{ref}, in GW), and the value of α_{r} used to determine reserve capacities. The experiments consider test cases with up to 30,000 buses, significantly larger than almost all previous works. Large systems have a smaller value of α_{r} because they contain significantly more generators, whereas the size of the largest generator typically remains in the same order of magnitude. For every test case, 50,000 instances are generated and solved using Gurobi. This dataset is then split into training, validation, and test sets which comprise 40000, 5000, and 5000 instances.

B. Baseline Models

The proposed end-to-end learning and repair model (E2ELR) is evaluated against four architectures. First, a naive, fully-connected DNN model without any feasibility layer (DNN). This model only includes a sigmoid activation layer to enforce generation bounds (constraint (1e)). Second, a fully-connected DNN model with the DeepOPF architecture [7] (DeepOPF). It uses an equality completion to ensure the satisfaction of equality constraints; the output may violate inequality constraints. Third, a fully-connected DNN model with the DC3 architecture [17] (DC3). This architecture uses a fixed-step unrolled gradient descent to minimize constraint violations; it is however not guaranteed to reach zero violations. Note that the DC3 architecture requires a significant amount of hypertuning to achieve decent results. The last model is a fully-connected DNN model, combined with the LOOP-LC architecture from [39] (LOOP). The gauge mapping used in LOOP does not support the compact form of (9), therefore it is not included in the ED-R experiments. These baseline models are detailed in [44].

All baselines use a fully-connected DNN architecture, with the main difference being how feasibility is handled. Graph Neural Network (GNN) architectures are not considered in this work, as they were found to be numerically less stable and exhibited poorer performance than DNNs in preliminary experiments. Nevertheless, note that the proposed repair layers can also be used in conjunction with a GNN architecture.

C. Performance Metrics

The performance of each ML model is evaluated with respect to several metrics that measure both accuracy and computational efficiency. Given an instance $\mathbf{x}$ with optimal solution $\mathbf{p}^*$ and a predicted solution $\hat{\mathbf{p}}$, the optimality gap is defined as gap $= (\hat{Z} - Z^*) \times |Z^*|^{-1}$, where Z^* is the optimal value of the problem, and $\hat{Z}$ is the objective value of the prediction, plus a penalty for hard constraint violations, i.e.,

$$c(\hat{\mathbf{p}}) + M_{\text{th}} \|\xi_{\text{th}}(\hat{\mathbf{p}})\|_1 + M_{\text{pb}} |\mathbf{e}^\top (\hat{\mathbf{p}} - \mathbf{d})| + M_{\text{r}} \xi_{\text{r}}(\hat{\mathbf{p}}), \quad (19)$$

where $\xi_{\text{r}}(\hat{\mathbf{p}})$ is defined as in function (15). Penalizing hard constraint violations is necessary to ensure a fair comparison between models that output feasible solutions and those that do not. Because all considered models enforce constraints (1d)–(1f), they are not penalized in (19).

The article uses realistic penalty prices, based on the values used by MISO in their operations [48], [49]. Namely, the thermal violation penalty price M_{th} is set to \$1500/MW. The power balance violation penalty M_{pb} is set to \$3500/MW, which corresponds to MISO's value of lost load (VOLL). Finally, the reserve shortage penalty M_{r} is set to \$1100/MW, which is MISO's reserve shortage price. The ability of optimization proxies to output feasible solution is measured via the proportion of feasible predictions, which is reported as a percentage over the test set. The article uses an absolute tolerance of 10^{-4} p.u. to decide whether a constraint is violated; note that this is 100x larger than the default absolute tolerance of optimization solvers. The article also reports the mean constraint violation of infeasible predictions.

TABLE II
MEAN OPTIMALITY GAP (%) ON TEST SET

		ED					ED-R			
Loss	System	DNN	E2ELR	DeepOPF	DC3	LOOP	DNN	E2ELR	DeepOPF	DC3
SL	`ieee300`	69.55	**1.42**	2.81	3.03	38.93	75.06	**1.52**	2.80	2.94
	`pegase1k`	48.77	**0.74**	7.78	2.80	32.53	47.84	**0.74**	7.50	2.97
	`rte6470`	55.13	**1.35**	28.23	3.68	50.21	70.57	**1.82**	46.66	3.49
	`pegase9k`	76.06	**0.38**	33.20	1.25	33.78	81.19	**0.38**	30.84	1.29
	`pegase13k`	71.14	**0.29**	64.93	1.79	52.94	76.32	**0.28**	69.23	1.81
	`goc30k`	194.13	**0.46**	55.91	2.75	36.49	136.25	**0.45**	41.34	2.35
SSL	`ieee300`	35.66	**0.74**	2.23	2.51	37.78	45.56	**0.78**	2.82	2.80
	`pegase1k`	62.07	**0.63**	10.83	2.57	32.20	64.69	**0.68**	9.83	2.61
	`rte6470`	40.73	**1.30**	42.28	2.82	50.20	55.16	**1.68**	48.57	3.04
	`pegase9k`	43.68	**0.32**	34.33	0.82	33.76	44.74	**0.29**	42.06	0.93
	`pegase13k`	57.58	**0.21**	60.12	0.84	52.93	61.28	**0.19**	65.38	0.91
	`goc30k`	108.91	**0.39**	8.39	0.72	36.73	93.91	**0.33**	9.47	0.71

TABLE III
POWER BALANCE CONSTRAINT VIOLATION STATISTICS

		ED						ED-R					
		DNN		DeepOPF		DC3		DNN		DeepOPF		DC3	
Loss	System	%feas	viol	%feas	viol	%feas	viol	%feas	viol	%feas	viol	%feas	viol
SL	`ieee300`	0%	0.50	100%	0.00	100%	0.00	0%	0.70	100%	0.06	100%	0.25
	`pegase1k`	0%	1.82	71%	1.35	65%	0.04	0%	1.90	70%	1.19	65%	0.08
	`rte6470`	0%	2.08	1%	1.94	9%	0.03	0%	2.26	1%	2.81	7%	0.01
	`pegase9k`	0%	6.25	3%	6.38	29%	0.00	0%	5.91	3%	5.99	29%	0.00
	`pegase13k`	0%	6.63	1%	7.08	23%	0.00	0%	7.79	1%	7.46	22%	0.00
	`goc30k`	0%	3.81	45%	1.70	57%	0.03	0%	2.31	54%	1.54	69%	0.00
SSL	`ieee300`	0%	0.58	100%	0.00	100%	0.16	0%	0.73	100%	0.56	100%	0.29
	`pegase1k`	0%	2.42	63%	2.56	63%	0.03	0%	2.30	63%	1.81	39%	0.05
	`rte6470`	0%	1.90	1%	2.64	6%	0.11	0%	2.72	1%	2.51	5%	0.01
	`pegase9k`	0%	7.22	3%	5.46	27%	0.05	0%	7.00	3%	7.87	25%	0.08
	`pegase13k`	0%	6.41	1%	7.19	19%	0.01	0%	6.82	1%	7.83	20%	0.01
	`goc30k`	0%	3.18	55%	1.24	52%	0.01	0%	2.61	49%	1.20	62%	0.02

†with 200 gradient steps. *geometric mean of non-zero violations, in p.u.

TABLE IV
SAMPLING AND TRAINING TIME COMPARISON (ED)

Loss	System	Sample	DNN	E2ELR	DeepOPF	DC3	LOOP
SL	`ieee300`	0.2 h	7 min	37 min	31 min	121 min	33 min
	`pegase1k`	0.7 h	8 min	14 min	6 min	41 min	19 min
	`rte6470`	5.1 h	11 min	30 min	13 min	73 min	18 min
	`pegase9k`	12.7 h	15 min	24 min	22 min	123 min	25 min
	`pegase13k`	20.6 h	14 min	19 min	14 min	126 min	19 min
	`goc30k`	63.4 h	25 min	20 min	41 min	108 min	127 min
SSL	`ieee300`	–	15 min	27 min	38 min	102 min	27 min
	`pegase1k`	–	8 min	15 min	11 min	46 min	14 min
	`rte6470`	–	9 min	17 min	10 min	42 min	15 min
	`pegase9k`	–	18 min	20 min	17 min	100 min	29 min
	`pegase13k`	–	17 min	18 min	14 min	125 min	15 min
	`goc30k`	–	38 min	45 min	51 min	105 min	60 min

Sampling (training) times are for 1 CPU (1 GPU). Excludes hypertuning.

The article also evaluates the computational efficiency of each ML model and learning paradigm (SL and SSL), as well as that of the repair layers. Computational efficiency is measured by (i) the training time of ML models, including the data-generation time when applicable, and (ii) the inference time. Note that ML models evaluate *batches* of instances, therefore, inference times are reported per batch of 256 instances. The performance of the repair layers presented in Section IV is benchmarked against a standard euclidean projection solved with state-of-the-art optimization software.

Unless specified otherwise, average computing times are arithmetic means; other averages are shifted geometric means

$$\mu_s(x_1, \ldots, x_n) = \exp\left(\frac{1}{n}\sum_i \log(x_i + s)\right) - s.$$

The article uses a shift s of 1% for optimality gaps, and 1p.u. for constraint violations.

D. Implementation Details

All optimization problems are formulated in Julia using JuMP [50], and solved with Gurobi 9.5 [51] with a single CPU thread and default parameter settings. All deep learning models are implemented using PyTorch [52] and trained using the Adam optimizer [53]. All models are hyperparameter tuned using a grid search, which is detailed in [44]. For each system, the best model is selected on the validation set and the performances on the test set are reported. During training, the learning rate is reduced by a factor of ten if the validation loss shows no improvement for a consecutive sequence of 10 epochs. In addition, training is stopped if the validation loss does not improve for consecutive 20 epochs. Experiments are conducted on dual Intel Xeon 6226@2.7 GHz machines running Linux, on the PACE Phoenix cluster [54]. The training of ML models is performed on Tesla V100-PCIE GPUs with 16GBs HBM2 RAM.

VII. NUMERICAL RESULTS

A. Optimality Gaps

Table II reports, for the ED and ED-R problems, the mean optimality gap of each ML model, under the SL and SSL learning modes. Bold entries denote the best-performing method. Recall that LOOP is not included in ED-R experiments. *E2ELR systematically outperforms all other baselines across all settings.* This stems from two reasons. First, DNN, DeepOPF and DC3 exhibit violations of the power balance constraint (1b), which yields high penalties and therefore large optimality gaps. Statistics on power balance violations for DNN, DeepOPF and DC3 are reported in Table III. Second, LOOP's poor performance, despite not violating any hard constraint, is because the non-convex gauge mapping used inside the model has an adverse impact on training. Indeed, after a few epochs of training, LOOP gets stuck in a local optimum.

E2ELR, when trained in a self-supervised mode, achieves the best performance. This is because SSL directly minimizes the true objective function, rather than the surrogate supervised loss. With the exception of `rte6470`, the performance of E2ELR improves as the size of the system increases, with the lowest optimality gaps achieved on `pegase13 k`, which has the most generators. Note that `rte6470`is a real system from the French transmission grid: it is more congested than other test cases, and therefore harder to learn.

B. Computing Times

Tables IV and V report the sampling and training times for ED and ED-R, respectively. Each table reports the total time for data-generation, which corresponds to the total solving time of Gurobi on a single thread. There is no labeling time for self-supervised models. While training times for SL and SSL are comparable, for a given architecture, the latter does not incur any labeling time. The training time of DC3 is significantly higher than other baselines because of its unrolled gradient steps. These results demonstrate that ML models can be trained efficiently on large-scale systems. Indeed, *the self-supervised E2ELR needs less than an hour of total computing time to achieve optimality gaps under 0.5% for systems with thousands of buses.*

TABLE V
SAMPLING AND TRAINING TIME COMPARISON (ED-R)

Loss	System	Sample	DNN	E2ELR	DeepOPF	DC3
SL	ieee300	0.2 h	12 min	43 min	43 min	115 min
	pegase1k	0.8 h	14 min	19 min	19 min	53 min
	rte6470	4.6 h	14 min	19 min	19 min	71 min
	pegase9k	14.0 h	15 min	22 min	22 min	123 min
	pegase13k	22.7 h	16 min	27 min	27 min	126 min
	goc30k	65.9 h	32 min	39 min	38 min	129 min
SSL	ieee300	–	21 min	37 min	37 min	131 min
	pegase1k	–	6 min	19 min	19 min	67 min
	rte6470	–	12 min	21 min	21 min	71 min
	pegase9k	–	20 min	24 min	24 min	123 min
	pegase13k	–	13 min	22 min	22 min	125 min
	goc30k	–	52 min	53 min	53 min	128 min

Sampling (training) times are for 1 CPU (1 GPU). Excludes hypertuning.

TABLE VI
SOLVING AND INFERENCE TIME COMPARISON (ED)

Loss	System	DNN	E2ELR	DeepOPF	DC3[†]	LOOP	GRB[*]
SL	ieee300	3.4 ms	4.5 ms	4.8 ms	15.4 ms	5.3 ms	12.1 ms
	pegase1k	4.1 ms	5.3 ms	4.3 ms	18.3 ms	5.9 ms	51.5 ms
	rte6470	5.1 ms	6.6 ms	5.4 ms	35.3 ms	7.1 ms	364.4 ms
	pegase9k	6.0 ms	7.3 ms	6.2 ms	91.5 ms	8.2 ms	913.5 ms
	pegase13k	7.3 ms	8.3 ms	8.7 ms	523.6 ms	13.9 ms	1481.3 ms
	goc30k	9.5 ms	10.0 ms	9.3 ms	443.0 ms	14.4 ms	4566.9 ms
SSL	ieee300	3.4 ms	6.0 ms	3.7 ms	15.1 ms	5.2 ms	12.1 ms
	pegase1k	4.0 ms	5.3 ms	4.3 ms	18.4 ms	5.8 ms	51.5 ms
	rte6470	5.9 ms	6.5 ms	6.3 ms	36.7 ms	9.5 ms	364.4 ms
	pegase9k	6.1 ms	7.0 ms	6.3 ms	93.2 ms	10.3 ms	913.5 ms
	pegase13k	7.1 ms	8.2 ms	7.2 ms	561.2 ms	12.8 ms	1481.3 ms
	goc30k	10.9 ms	11.7 ms	9.4 ms	444.2 ms	21.7 ms	4566.9 ms

[†]with 200 gradient steps. [*]solution time per instance (single thread).
All ML inference times are for a batch of 256 instances.

TABLE VII
SOLVING AND INFERENCE TIME COMPARISON (ED-R)

Loss	System	DNN	E2ELR	DeepOPF	DC3[†]	GRB[*]
SL	ieee300	3.9 ms	6.5 ms	4.6 ms	16.5 ms	12.6 ms
	pegase1k	4.5 ms	6.0 ms	4.8 ms	18.9 ms	56.5 ms
	rte6470	5.7 ms	10.4 ms	6.2 ms	36.1 ms	333.6 ms
	pegase9k	6.3 ms	7.7 ms	6.7 ms	91.6 ms	1008.0 ms
	pegase13k	8.3 ms	10.7 ms	8.8 ms	531.2 ms	1632.7 ms
	goc30k	9.3 ms	11.1 ms	10.6 ms	438.7 ms	4745.7 ms
SSL	ieee300	3.9 ms	7.6 ms	4.4 ms	17.6 ms	12.6 ms
	pegase1k	4.4 ms	5.9 ms	4.7 ms	19.1 ms	56.5 ms
	rte6470	6.4 ms	10.5 ms	6.7 ms	37.3 ms	333.6 ms
	pegase9k	7.1 ms	8.3 ms	7.2 ms	92.9 ms	1008.0 ms
	pegase13k	7.8 ms	8.9 ms	7.9 ms	522.4 ms	1632.7 ms
	goc30k	10.2 ms	12.4 ms	10.3 ms	435.8 ms	4745.7 ms

[†]with 200 gradient steps. [*]solution time per instance (single thread).
All ML inference times are for a batch of 256 instances.

TABLE VIII
COMPARISON OF OPTIMALITY GAPS (%) WITH AND WITHOUT FEASIBILITY RESTORATION (ED)

			DNN			DeepOPF			DC3		
Loss	System	E2ELR	–	FL	EP	–	FL	EP	–	FL	EP
SL	ieee300	**1.42**	69.55	36.33	36.37	2.81	2.81	2.81	3.03	3.03	3.03
	pegase1k	**0.74**	48.77	3.98	3.94	7.78	5.24	5.28	2.80	2.44	2.44
	rte6470	**1.35**	55.13	21.28	21.41	28.23	1.89	1.89	3.68	3.36	3.36
	pegase9k	**0.38**	76.06	34.61	34.65	33.20	1.94	1.99	1.25	1.24	1.24
	pegase13k	**0.29**	71.14	32.70	32.72	64.93	23.36	23.36	1.79	1.79	1.79
	goc30k	**0.46**	194.13	57.53	57.41	55.91	30.19	30.16	2.75	2.45	2.45
SSL	ieee300	**0.74**	35.66	3.82	3.73	2.23	2.23	2.23	2.51	2.51	2.51
	pegase1k	**0.63**	62.07	3.24	3.25	10.83	3.21	3.18	2.57	2.35	2.35
	rte6470	**1.30**	40.73	11.52	11.47	42.28	5.38	5.37	2.82	2.10	2.09
	pegase9k	**0.32**	43.68	3.20	3.22	34.33	4.73	4.74	0.82	0.64	0.64
	pegase13k	**0.21**	57.58	20.59	20.59	60.12	18.85	18.84	0.84	0.81	0.81
	goc30k	**0.39**	108.91	7.89	7.89	8.39	3.06	3.06	0.72	0.62	0.62

TABLE IX
COMPARISON OF OPTIMALITY GAPS (%) WITH AND WITHOUT FEASIBILITY RESTORATION (ED-R)

			DNN			DeepOPF			DC3		
Loss	System	E2ELR	–	FL	EP	–	FL	EP	–	FL	EP
SL	ieee300	**1.52**	75.06	30.47	30.49	2.80	2.80	2.80	2.94	2.94	2.94
	pegase1k	**0.74**	47.84	2.52	2.50	7.50	4.79	4.79	2.97	2.34	2.34
	rte6470	**1.82**	70.57	30.20	29.90	46.66	2.63	2.51	3.49	3.32	3.29
	pegase9k	**0.38**	81.19	41.34	41.40	30.84	1.90	1.92	1.29	1.29	1.29
	pegase13k	**0.28**	76.32	30.00	30.02	69.23	25.09	25.09	1.81	1.81	1.81
	goc30k	**0.45**	136.25	53.34	53.41	41.34	22.53	22.43	2.35	2.31	2.31
SSL	ieee300	**0.78**	45.56	4.50	4.34	2.82	2.79	2.79	2.80	2.78	2.78
	pegase1k	**0.68**	64.69	4.56	4.44	9.83	3.97	3.95	2.61	1.87	1.87
	rte6470	**1.68**	55.16	9.76	9.43	48.57	8.79	8.53	3.04	2.75	2.70
	pegase9k	**0.29**	44.74	4.33	4.33	42.06	2.28	2.30	0.93	0.66	0.66
	pegase13k	**0.19**	61.28	21.35	21.32	65.38	19.64	19.64	0.91	0.89	0.89
	goc30k	**0.33**	93.91	10.00	9.98	9.47	2.58	2.58	0.71	0.64	0.64

Tables VI and VII report, for ED and ED-R, respectively, the average solving time using Gurobi (GRB) and average inference times of ML methods. Recall that the Gurobi's solving times are for a single instance solved on a single CPU core, whereas the ML inference times are reported for a batch of 256 instances on a GPU. Also note that the number of gradient steps used by DC3 to recover feasibility is set to 200 for inference (compared to 50 for training).

On systems with more than 6,000 buses, DC3 is typically 10–30 times slower than other baselines, again due to its unrolled gradient steps. In contrast, DNN, DeepOPF, E2ELR, and LOOP all require in the order of 5–10 milliseconds to evaluate a batch of 256 instances. For the largest systems, this represents about 25,000 instances per second, on a single GPU. Solving the same volume of instances with Gurobi would require more than a day on a single CPU. Getting this time down to the order of seconds, thereby matching the speed of ML proxies, would require thousands of CPUs, which comes at high financial and environmental costs.

C. *Benefits of End-to-End Training*

Tables VIII and IX further demonstrate the benefits of training end-to-end feasible models: they report, for ED and ED-R problems, the optimality gaps achieved by DNN, DeepOPF and DC3 *after applying a repair step at inference time*. Two repair mechanisms are compared: the proposed Repair Layers (RL) and a Euclidean Projection (EP). The tables also report the mean gap achieved by E2ELR as a reference baseline. The results can be summarized as follows. First, the additional feasibility restoration improves the quality of the initial prediction. This is especially true for DNN and DeepOPF, which exhibited the largest constraint violations (see Table III): optimality gaps are improved by a factor 2–20, but remain very high nonetheless. Second, the two repair mechanisms yield similar optimality gaps. For DC3, there is virtually no difference between RL and EP. Third, across all experiments, even after feasibility restoration, E2ELR remains the best-performing model, with optimality gaps 2–6x smaller than DC3. Table X compares the computing times of the feasibility restoration using either the repair layers (RL) or the euclidean projection (EP). The latter is solved as a quadratic program with Gurobi. All benchmarks are conducted in Julia on a single thread, using the `BenchmarkTools` utility [55], and median times are reported. The results of Table X show that evaluating the proposed repair layers is three orders of magnitude faster than solving the euclidean projection problem.

TABLE X
COMPUTING TIME OF FEASIBILITY RESTORATION USING FEASIBILITY LAYERS (FL) AND EUCLIDEAN PROJECTION (EP)

Problem	System	RL	EP	Speedup
ED	`ieee300`	0.13 µs	0.45 ms	3439x
	`pegase1k`	0.55 µs	1.41 ms	2572x
	`rte6470`	1.40 µs	3.75 ms	2686x
	`pegase9k`	2.37 µs	6.90 ms	2911x
	`pegase13k`	6.42 µs	20.71 ms	3227x
	`goc30k`	5.67 µs	17.87 ms	3155x
ED-R	`ieee300`	1.06 µs	1.00 ms	939x
	`pegase1k`	4.58 µs	3.42 ms	748x
	`rte6470`	10.46 µs	10.19 ms	974x
	`pegase9k`	20.14 µs	18.38 ms	913x
	`pegase13k`	42.67 µs	60.73 ms	1423x
	`goc30k`	39.80 µs	49.17 ms	1236x

Median computing times as measured by `BenchmarkTools`

VIII. CONCLUSION

The article proposed a new *End-to-End Learning and Repair* (E2ELR) architecture for training optimization proxies for economic dispatch problems. E2ELR combines deep learning with closed-form, differential repair layers, thereby integrating prediction and feasibility restoration in an end-to-end fashion. The E2ELR architecture can be trained with self-supervised learning, removing the need for labeled data and the solving of numerous optimization problems offline. The article conducted extensive numerical experiments on the ecocomic dispatch of large-scale, industry-size power grids with tens of thousands of buses. It also presented the first study that considers reserve requirements in the context of optimization proxies, reducing the gap between academic and industry formulations. The results demonstrate that the combination of E2ELR and self-supervised learning achieves state-of-the-art performance, with optimality gaps that outperform other baselines by at least an order of magnitude. Future research will investigate security-constrained economic dispatch (SCED) formulations, and the extension of repair layers to thermal constraints, multi-period settings and the nonlinear, non-convex AC-OPF.

REFERENCES

[1] MISO, "Energy and operating reserve markets," Business Practices Manual Energy and Operating Reserve Markets, 2022.
[2] Midcontinent ISO, "MISO's response to the reliability imperative," 2023. [Online]. Available: https://cdn.misoenergy.org/MISO%20Response%20to%20the%20Reliability%20Imperative504018.pdf
[3] O. Stover, P. Karve, and S. Mahadevan, "Reliability and risk metrics to assess operational adequacy and flexibility of power grids," *Rel. Eng. Syst. Saf.*, vol. 231, 2023, Art. no. 109018.
[4] O. Stover et al., "Just-in-time learning for operational risk assessment in power grids," 2022, *arXiv:2209.12762*.
[5] W. Chen, S. Park, M. Tanneau, and P. V. Hentenryck, "Learning optimization proxies for large-scale security-constrained economic dispatch," *Electric Power Syst. Res.*, vol. 213, 2022, Art. no. 108566.
[6] Y. Ng, S. Misra, L. A. Roald, and S. Backhaus, "Statistical learning for DC optimal power flow," in *Proc. IEEE Power Syst. Comput. Conf.*, 2018, pp. 1–7.
[7] X. Pan, T. Zhao, M. Chen, and S. Zhang, "DeepOPF: A deep neural network approach for security-constrained DC OPF," *IEEE Trans. Power Syst.*, vol. 36, no. 3, pp. 1725–1735, May 2021.
[8] R. Nellikkath and S. Chatzivasileiadis, "Physics-informed neural networks for minimising worst-case violations in DC optimal power flow," in *Proc. IEEE Int. Conf. Commun., Control, Comput. Technol. Smart Grids*, 2021, pp. 419–424.
[9] T. Zhao, X. Pan, M. Chen, and S. Low, "Ensuring DNN solution feasibility for optimization problems with linear constraints," in *Proc. 11th Int. Conf. Learn. Representations*, 2023.
[10] A. Stratigakos, S. Pineda, J. M. Morales, and G. Kariniotakis, "Interpretable machine learning for DC optimal power flow with feasibility guarantees," Working Paper or Preprint, Mar. 2023. [Online]. Available: https://hal.science/hal-04038380
[11] R. Ferrando et al., "A physics-informed machine learning for electricity markets: A NYISO case study," 2023, *arXiv.2304.00062*.
[12] N. Guha, Z. Wang, M. Wytock, and A. Majumdar, "Machine learning for AC optimal power flow," 2019, *arXiv:1910.08842*.
[13] A. S. Zamzam and K. Baker, "Learning optimal solutions for extremely fast AC optimal power flow," in *Proc. IEEE Int. Conf. Commun., Control, Comput. Technol. Smart Grids*, 2020, pp. 1–6.
[14] D. Owerko, F. Gama, and A. Ribeiro, "Optimal power flow using graph neural networks," in *Proc. IEEE Int. Conf. Acoust., Speech, Signal Process.*, 2020, pp. 5930–5934.
[15] F. Fioretto, T. W. Mak, and P. V. Hentenryck, "Predicting AC optimal power flows: Combining deep learning and Lagrangian dual methods," in *Proc. AAAI Conf. Artif. Intell.*, 2020, pp. 630–637.
[16] M. Chatzos, T. W. Mak, and P. V. Hentenryck, "Spatial network decomposition for fast and scalable AC-OPF learning," *IEEE Trans. Power Syst.*, vol. 37, no. 4, pp. 2601–2612, Jul. 2022.
[17] P. Donti, D. Rolnick, and J. Z. Kolter, "DC3: A learning method for optimization with hard constraints," in *Proc. Int. Conf. Learn. Representations*, 2021.
[18] R. Nellikkath and S. Chatzivasileiadis, "Physics-informed neural networks for AC optimal power flow," *Electric Power Syst. Res.*, vol. 212, 2022, Art. no. 108412.
[19] X. Pan, M. Chen, T. Zhao, and S. H. Low, "DeepOPF: A feasibility-optimized deep neural network approach for AC optimal power flow problems," *IEEE Syst. J.*, vol. 17, no. 1, pp. 673–683, Mar. 2023.
[20] X. Pan, W. Huang, M. Chen, and S. H. Low, "DeepOPF-AL: Augmented learning for solving AC-OPF problems with a multi-valued load-solution mapping," in *Proc. 14th ACM Int. Conf. Future Energy Syst.*, 2023, pp. 42–47.
[21] M. Zhou, M. Chen, and S. H. Low, "DeepOPF-FT: One deep neural network for multiple AC-OPF problems with flexible topology," *IEEE Trans. Power Syst.*, vol. 38, no. 1, pp. 964–967, Jan. 2023.
[22] S. Liu, C. Wu, and H. Zhu, "Topology-aware graph neural networks for learning feasible and adaptive AC-OPF solutions," *IEEE Trans. Power Syst.*, early access, Dec. 19, 2022, doi: 10.1109/TPWRS.2022.3230555.
[23] T. Falconer and L. Mones, "Leveraging power grid topology in machine learning assisted optimal power flow," *IEEE Trans. Power Syst.*, vol. 38, no. 3, pp. 2234–2246, May 2023.
[24] D. Owerko, F. Gama, and A. Ribeiro, "Unsupervised optimal power flow using graph neural networks," 2022, *arXiv:2210.09277*.
[25] T. Pham and X. Li, "Reduced optimal power flow using graph neural network," in *Proc. IEEE North Amer. Power Symp.*, 2022, pp. 1–6.
[26] M. Gao, J. Yu, Z. Yang, and J. Zhao, "A physics-guided graph convolution neural network for optimal power flow," *IEEE Trans. Power Syst.*, early access, Jan. 20, 2023, doi: 10.1109/TPWRS.2023.3238377.
[27] S. Park, W. Chen, T. W. Mak, and P. V. Hentenryck, "Compact optimization learning for AC optimal power flow," 2023, *arXiv:2301.08840*.
[28] M. Mitrovic et al., "Data-driven stochastic AC-OPF using Gaussian process regression," *Int. J. Elect. Power Energy Syst.*, vol. 152, 2023, Art. no. 109249.
[29] S. Gupta, S. Misra, D. Deka, and V. Kekatos, "DNN-based policies for stochastic AC OPF," *Electric Power Syst. Res.*, vol. 213, 2022, Art. no. 108563.
[30] M. Klamkin, M. Tanneau, T. W. K. Mak, and P. V. Hentenryck, "Active bucketized learning for ACOPF optimization proxies," 2022, *arXiv:2208.07497*.
[31] Z. Hu and H. Zhang, "Optimal power flow based on physical-model-integrated neural network with worth-learning data generation," 2023, *arXiv:2301.03766*.
[32] W. Huang and M. Chen, "DeepOPF-NGT: Fast no ground truth deep learning-based approach for AC-OPF problems," in *Proc. Workshop Tackling Climate Change With Mach. Learn.*, 2021. [Online]. Available: https://www.climatechange.ai/papers/icml2021/18
[33] J. Wang and P. Srikantha, "Fast optimal power flow with guarantees via an unsupervised generative model," *IEEE Trans. Power Syst.*, vol. 38, no. 5, pp. 4593–4604, Sep. 2023.

[34] S. Park and P. V. Hentenryck, “Self-supervised primal-dual learning for constrained optimization,” in *Proc. AAAI Conf. Artif. Intell.*, 2023, pp. 4052–4060.

[35] A. Venzke and S. Chatzivasileiadis, “Verification of neural network behaviour: Formal guarantees for power system applications,” *IEEE Trans. Smart Grid*, vol. 12, no. 1, pp. 383–397, Jan. 2021.

[36] B. Taheri and D. K. Molzahn, “Restoring AC power flow feasibility from relaxed and approximated optimal power flow models,” in *Proc. Amer. Control Conf.*, 2023, pp. 4463–4470.

[37] A. Agrawal, B. Amos, S. Barratt, S. Boyd, S. Diamond, and J. Z. Kolter, “Differentiable convex optimization layers,” in *Proc. Int. Conf. Adv. Neural Inf. Process. Syst.*, 2019.

[38] M. Kim and H. Kim, “Projection-aware deep neural network for DC optimal power flow without constraint violations,” in *Proc. IEEE Int. Conf. Commun., Control, Comput. Technol. Smart Grids*, 2022, pp. 116–121.

[39] M. Li, S. Kolouri, and J. Mohammadi, “Learning to solve optimization problems with hard linear constraints,” *IEEE Access*, vol. 11, pp. 59995–60004, 2023.

[40] C. Josz, S. Fliscounakis, J. Maeght, and P. Panciatici, “AC power flow data in MATPOWER and QCQP format: ITesla, RTE snapshots, and PEGASE,” 2016, *arXiv:1603.01533*.

[41] J. Holzer, Y. Chen, Z. Wu, F. Pan, and A. Veeramany, “Fast simultaneous feasibility test for security constrained unit commitment,” *IEEE Trans. Power Syst.*, early access, pp. 1–10, Apr. 06, 2023, doi: 10.1109/TPWRS.2023.3265269.

[42] X. Ma, H. Song, M. Hong, J. Wan, Y. Chen, and E. Zak, “The security-constrained commitment and dispatch for midwest ISO day-ahead co-optimized energy and ancillary service market,” in *Proc. IEEE Power Energy Soc. Gen. Meeting*, 2009, pp. 1–8.

[43] MISO, “Real-time energy and operating reserve market software formulations and business logic,” Business Practices Manual Energy and Operating Reserve Markets Attachment D, 2022.

[44] W. Chen, M. Tanneau, and P. V. Hentenryck, “End-to-end feasible optimization proxies for large-scale economic dispatch,” 2023, *arXiv:2304.11726*.

[45] S. Babaeinejadsarookolaee et al., “The power grid library for benchmarking AC optimal power flow algorithms,” 2019, *arXiv:1908.02788*.

[46] “Power systems test case archive,” Dept. of Elect. Eng., University of Washington, 1999. [Online]. Available: http://www.ee.washington.edu/research/pstca/

[47] Grid Optimization Competition, “Grid optimization competition datasets,” 2018. [Online]. Available: https://gocompetition.energy.gov/

[48] MISO, “Schedule 28–Demand curves for toperating reserves,” 2023. [Online]. Available: https://www.misoenergy.org/legal/tariff/

[49] MISO, “Schedule 28A–demand curves for transmission constraints,” 2019. [Online]. Available: https://www.misoenergy.org/legal/tariff/

[50] I. Dunning‘, J. Huchette, and M. Lubin, “Jump: A modeling language for mathematical optimization,” *SIAM Rev.*, vol. 59, no. 2, pp. 295–320, 2017.

[51] Gurobi Optimization, LLC, “Gurobi optimizer reference manual,” 2023. [Online]. Available: https://www.gurobi.com

[52] A. Paszke et al., “Automatic differentiation in Pytorch,” in *Proc. Int. Conf. Adv. Neural Inf. Process. Syst.-Workshops*, 2017.

[53] D. P. Kingma and J. Ba, “Adam: A method for stochastic optimization,” in *Proc. 3rd Int. Conf. Learn. Representations*, 2015.

[54] PACE, “Partnership for an advanced computing environment (PACE),” 2017. [Online]. Available: http://www.pace.gatech.edu

[55] J. Chen and J. Revels, “Robust benchmarking in noisy environments,” Aug. 2016, *arXiv:1608.04295*.

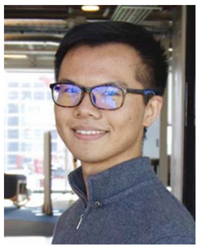

Wenbo Chen (Student Member, IEEE) received the B.S. degree in electrical engineering from the Huazhong University of Science and Technology, Wuhan, China, in 2019. He is currently working toward the Ph.D. degree in machine learning with the Georgia Institute of Technology, Atlanta, GA, USA. His research interests include fusing machine learning and optimization into large-scale, intelligent systems with applications in energy systems and supply chains.

Mathieu Tanneau received the M.Sc. degree from Ecole polytechnique, Palaiseau, France, and the Ph.D. degree from Polytechnique Montreal, Montreal, QC, Canada. He is currently a Research Engineer with the Georgia Institute of Technology, Atlanta, GA, USA. His research focuses on the combination of optimization and machine learning, with applications to power systems operations.

Pascal Van Hentenryck (Member, IEEE) is currently the A. Russell Chandler III Chair and a Professor with the H. Milton Stewart School of Industrial and Systems Engineering, Georgia Institute of Technology, Atlanta, GA, USA, and the Associate Chair for Innovation and Entrepreneurship. He is also the Director of the NSF AI for Advances in Optimization. His research interests include machine learning, optimization, and with applications in energy and supply chains. He is an INFORMS Fellow and a Fellow of the Association for the Advancement of Artificial Intelligence. He was the recipient of two honorary Doctoral degrees, and teaching excellence awards at Brown University and Georgia Tech. Several of his optimization systems have been in commercial use for more than 20 years.